www.sciencemag.org/cgi/content/full/science.1220683/DC1

Supplementary Materials for

Conformational Control of the Ste5 Scaffold Protein Insulates Against MAP Kinase Misactivation

Jesse G. Zalatan, Scott M. Coyle, Saravanan Rajan, Sachdev S. Sidhu, Wendell A. Lim*

*To whom correspondence should be addressed. E-mail: lim@cmp.ucsf.edu

Published 9 August 2012 on *Science* Express
DOI: 10.1126/science.1220683

This PDF file includes:

Materials and Methods

Yeast Strain Construction and Manipulation

The parent yeast strain for all experiments was F1950 (Σ1278b; *MAT***a** *ura3 leu2 trp1 his3*) (1). Strains derived from the Σ1278b lineage exhibit a haploid invasive growth phenotype (2-4). Yeast knockout strains were prepared using PCR-mediated gene deletion (5, 6), and transformations were performed with the lithium acetate method (7).

Expression constructs were integrated in single copies into the yeast genome using a set of custom-designed vectors (gifts from N. Helman and S. Vidal). These vectors consist of a multiple cloning site to introduce a promoter and ORF, the *Candida albicans* Adh1 terminator, auxotrophic complementation markers from *Candida glabrata* or *Candida albicans*, and 5' and 3' flanking homology regions (~500 bp) to target the corresponding auxotrophic locus (603, His3; 604, Trp1; Leu2; 606, Ura3). Prior to transformation, the vector is linearized by restriction digestion at sites just outside of the 5' and 3' flanking homology regions. Using this approach, only a single copy of the target gene is introduced into the yeast genome, unlike the pRS300 series of vectors (8), which can integrate multiple copies. Yeast strains and plasmids used in this work are listed in Tables S2 and S3. All constructs were expressed from their native promoters except the following: Ste11ΔN was overexpressed from the Adh1 promoter and Ste7EE was overexpressed from the Gal10 promoter (in experiments with Ste7EE, Ste5 and $Ste5_{VWA-C}$ were overexpressed from Adh1 promoters, fig. S8).

For analysis of MAPK phosphorylation in yeast subjected to starvation, yeast cells were grown in YPD (yeast peptone dextrose) liquid cultures to mid-log phase (OD_{600} 0.4-0.6). 250 μL of cells were plated on YPD and incubated at 30 °C for 18 hours (the yeast extract in YPD stimulates the invasive growth response (4)). Similar results were obtained when cells growing on YPD plates were streaked onto fresh YPD plates and incubated at 30 °C for 18 hours. Unstarved cells were obtained by streaking cells growing on SCD (synthetic complete dextrose) plates onto fresh SCD plates and incubating at 30 °C for 18 hours. Approximately 10 mg of cells were harvested directly from the plates. Yeast lysates were prepared using an alkaline lysis extraction (9). Samples were run on Novex 10% Tris-glycine gels (Life Technologies) to separate Fus3 and Kss1, and transferred to nitrocellulose membranes (Whatman Protran BA83). Western blots were carried out using a primary anti-phospho p44/p42 MAPK antibody (Cell Signaling Technology #4370) and a secondary IRDye 800CW Goat Anti-Rabbit IgG antibody (Li-Cor #926-32211) with Li-Cor Odyssey Blocking Buffer. Phosphoglycerate kinase (PGK) was used as a loading control with a primary anti-PGK antibody (Life Technologies #459250) and a secondary IRDye 680LT Goat Anti-Mouse IgG antibody (Li-Cor #926-68020). Blots were visualized using the Li-Cor Odyssey Imaging System.

For α-factor induction experiments, yeast cells were grown in YPD liquid cultures to mid-log phase (OD_{600} 0.4-0.6). 10 mL liquid cultures were treated with 2 μM α-factor (final concentration), incubated at 30 °C for 15 minutes, centrifuged at 1600g for 2 minutes at 4 °C, and frozen in liquid nitrogen. Yeast lysates were prepared and western blots were performed as described above for starvation assays.

The yeast invasive growth phenotype (2-4) was assayed by growing yeast strains in liquid cultures (YPD or SCD) to OD_{600} 0.4-0.6, then spotting 20 μL onto YPD (+ starvation) or SCD (- starvation) plates and incubating for 1-2 days at 30 °C. Yeast

extract in the YPD medium stimulates the invasive growth response (4). Invasive growth was assayed by washing under a stream of tap water.

For galactose inductions, yeast cells were grown in SCS (synthetic complete sucrose) media to OD_{600} 0.2, then induced with 2% galactose (final concentration), incubated at 30 °C for 4 hours, centrifuged at 1600g for 2 minutes at 4 °C, and frozen in liquid nitrogen. Yeast lysates were prepared and western blots were performed as described above for starvation assays.

Quantitative and qualitative (patch) yeast mating assays were performed in YPD media as described (10) using a *MAT*α *his1* mating tester (1). Quantitative mating efficiency was calculated from the titer of **a**/α cells divided by the titer of **a** cells.

Protein Expression and Purification

Constructs to express recombinant proteins were from previous work (11) or were generated by standard molecular biology methods. We used a catalytically-dead allele of Fus3 (K42R) in order to eliminate background autophosphorylation that is observed with the wild-type protein. For kinetic characterization, Ste5 constructs were expressed as maltose binding protein (MBP) fusions.

Fus3 and Ste5 constructs were expressed in Rosetta (DE3) pLysS *E. coli* cells by inducing with 0.5 mM IPTG overnight at 18 °C. Fus3 K42R was expressed using the pBH4 vector, a derivative of pET15 (Novagen) that was modified to produce an N-terminal His_6-tagged, TEV-cleavable protein. Full length Ste5 and truncation mapping constructs were expressed with an N-terminal TEV-cleavable MBP and a C-terminal His-tag. For Ste5Δ(544-592) and all other internal truncations (Fig. 3A and fig. S9), the deleted residues were replaced with a 5X(GAGS) linker. Ste5-ms (the minimal VWA domain, residues 593-786), the Ste5 PH domain fragment (Fig. 3E), and the $Ste5_{582-786}$ fragment used for crystallography were expressed from the pBH4 vector.

Constructs expressed from pBH4 were affinity purified on Ni-NTA (Qiagen), cleaved with TEV protease to release the N-terminal His_6 tag, and further purified by ion exchange (RESOURCE 15Q [Amersham], 20 mM Tris·HCl pH 8.0, 2 mM DTT, 10% glycerol, and 0-1 M NaCl). Constructs expressed from pMBP were affinity purified on Ni-NTA (Qiagen), followed by amylose resin (New England Biolabs). Purified proteins were dialyzed into 20 mM Tris Tris·HCl pH 8.0, 150 mM NaCl, 10% glycerol, and 2 mM DTT at 4 °C, aliqouted and stored at -80 °C.

Ste7 (constitutively active Ste7EE, bearing S359E and T363E phosphomimic mutations in the activation loop (11, 12)) and Ste11 (wild type) were expressed with an N-terminal TEV-cleavable MBP and C-terminal His-tag in *Spodoptera frugiperda* (SF9) cells, using the Bac-to-Bac Baculoviral Expression System (Life Technologies) at 27 °C. Proteins were affinity purified on Ni-NTA (Qiagen), followed by amylose resin (New England Biolabs). Purified proteins were dialyzed into 20 mM Tris Tris·HCl pH 8.0, 300 mM NaCl, 10% glycerol, and 2 mM DTT at 4 °C, aliqouted and stored at -80 °C. Prior work expressed Ste7 constructs with an N-terminal GST tag (11). In this work, we switched to an MBP tag to obtain higher purity protein and to eliminate any potential artifacts from GST dimerization (13, 14). MBP-Ste7EE and GST-Ste7EE were found to

have a similar k_{cat} for Fus3 phosphorylation (in reactions with Ste5),[1] and the K_{act} for Ste5 binding was ~5-fold weaker for MBP-Ste7EE than for GST-Ste7EE.[2] In the previous work, a variant of Ste7 with a single docking site for Fus3 was used (mutant Ste7EE-ND2 has the second, weaker docking site removed (15)). There was no difference in the behavior of Ste7EE and Ste7EE-ND2 for the kinetic parameters reported in this work.

Selection of a Ste5 PH Domain-Specific Fab

A minimal PH domain construct of Ste5 ($Ste5_{367-525}$) was expressed as a GST fusion protein with a C-terminal His-tag and affinity purified on Ni-NTA (Qiagen), followed by glutathione agarose (Sigma). As a negative control for selection, free GST with the C-terminal His tag (GST_{His}) was also purified as above.

We used a phage-displayed scFv library with a diversity of greater than 10^{11} unique clones and randomized at all 6 complementarity determining regions (CDRs). The library was built from an scFv scaffold that binds *E. coli* maltose binding protein, using methods previously described (16). Selection of domain-specific scFv sequences was performed as described (17). Briefly, 96-well Maxisorp Immunoplates (Fisher Scientific) were coated with 5 μg/mL GST-tagged $Ste5_{367-525}$ or GST_{His} in phosphate buffered saline (PBS). At each round of selection, phage that bound non-specifically were cleared by incubation on GST_{His} and unbound phage was transferred to the antigen-coated wells and allowed to incubate for 2 hours at room temperature. Wells were washed 10 times with PBS + 0.05% Tween-20. Bound phage was eluted with 0.1 N HCl and neutralized with 1 M Tris·HCl (pH 8.0) and used to infect actively growing *E. coli* XL1-Blue cells (Agilent Technologies) for overnight propagation. After five rounds of selection, phage particles were produced from individual clones and used in phage ELISAs to detect specifically binding clones. Positive clones were sequenced and the CDRs for unique clones were grafted onto an IPTG-inducible Fab scaffold using previously described methods (18).

The SR13 Fab protein was expressed in *E. coli* 55244 cells in 2YT with 100 μg/mL carbenicillin. Cells were grown to OD_{600} 0.8 before inducing with 1 mM IPTG for 16 h at 30 °C. Cells were resuspended in lysis buffer (1 mg/mL lysozyme, 37.5 U/mL benzonase, 2 mM $MgCl_2$, 0.2 mM PMSF) and incubated on ice for 1 h. The crude lysate was spun down and the supernatant was applied to an rProtein A affinity column (GE Healthcare), washed with 25 column volumes of PBS, eluted with elution buffer (50 mM NaH_2PO_4, 100 mM H_3PO_4, 140 mM NaCl, pH 2.0), and neutralized with neutralization buffer (1 M Na_2HPO_4, 140 mM NaCl, pH 8.6). Purified protein was concentrated and buffer exchanged to PBS on Amicon Ultracel 10K filter units (Millipore).

In Vitro Kinetic Assays

In vitro kinetic assays were conducted in 25 mM Tris·HCl (pH 8.0), 100 mM NaCl, 2.5 mM $MgCl_2$, 0.05% IGEPAL, and 2 mM TCEP at 25 °C. Fus3 phosphorylation reactions were initiated by addition of ATP to a final concentration of 500 μM.

---

[1] The value of k_{cat} for phosphorylation of Fus3 in the absence of Ste5 was approximately 10-fold faster for MBP-Ste7EE (Fig. S2) than for GST-Ste7EE-ND2 (11).

[2] The reported value of K_{act} in this work of 125 nM measured with MBP-Ste7EE and $Ste5_{VWA-C}$ is coincidentally similar to the value of 161 nM measured with GST-Ste7EE-ND2 and Ste5-ms reported previously (11) because the ~5-fold weaker binding by MBP-Ste7EE is compensated by the ~5-fold stronger binding to a Ste5 construct that has the complete Ste7 binding site (see fig. S4).

To determine the rate of Ste7 dissociation from Ste5 (k_{off}), 100 nM Ste5, 100 nM Ste11, 100 nM Ste7EE, and 500 nM Fus3 K42R were pre-incubated in reaction buffer on ice. Dissociation reactions were initiated by introducing a large excess (20 μM) of a Ste7 binding domain (the "sink", a minimal Ste7 binding domain from Ste5 [residues 759-810]), which captures Ste7 as it dissociates from Ste5. After varying times, ATP was added, and reaction timepoints were collected at 15 second intervals by quenching in 4X LDS sample loading buffer (Life Technologies) supplemented with 50 mM EDTA and 2 mM DTT and placing the samples in a boiling heat block (>100 °C) for 90 seconds. Samples were run on NuPAGE 4-12% Bis-Tris gels (Life Technologies) and transferred to nitrocellulose membranes (Whatman Protran BA83).

Quantitative western blots were carried out using a primary anti-phospho p44/p42 MAPK antibody (Cell Signaling Technology #4370) and a secondary IRDye 800CW Goat Anti-Rabbit IgG antibody (Li-Cor #926-32211) using 5% milk as a blocking solution. Blots were visualized using the Li-Cor Odyssey Imaging System and quantified using Odyssey 2.1 software as described previously (11).

Kinetic parameters and their standard errors were determined by nonlinear least-squares fitting to initial rate data. The initial rate of Fus3 phosphorylation at each timepoint after addition of the Ste7 binding domain sink corresponds to the amount of Ste5-Ste7-Fus3 complex remaining at each timepoint. k_{off} was determined by fitting to the equation $V_{obs} = V_0 \cdot e^{-k_{off} \cdot t} + C$, where t is the time after addition of the sink, V_0 is the initial rate without any sink added and C is a constant to account for weak residual activity due to incomplete capture of Ste7 by the sink. The observed k_{off} of 0.2 s^{-1} is a lower limit – dissociation occurs on a timescale faster than can be measured with mixing by hand. No change in dissociation rates was observed in the presence or absence of Ste11 (Fig. S1).

To determine steady state rate constants (k_{cat} and K_M), the concentration of Fus3 K42R was varied from 10 nM to 1 μM at a constant, saturating concentration of 1 μM Ste5. To determine K_{act}, the concentration of Ste5 was varied from 10 nM to 3 μM at a constant, saturating concentration of 500 μM Fus3 K42R. Reactions were typically conducted at 50 nM Ste7EE. In separate experiments, the concentration of Ste7EE was varied over a >10-fold range from 20-250 nM to confirm that reaction rates scaled linearly with total enzyme concentration.

Plots of V_{obs} vs. [Fus3] were fit to the Michaelis-Menten equation ($V_{obs} = k_{cat}[E]_0[S]/(K_M+[S])$) where $[E]_0$ is the total Ste7EE concentration and [S] is the Fus3 concentration. To determine K_{act}, plots of V_{obs} vs. [Ste5] were fit to a simple binding equation ($V_{obs} = k_{cat}[E]_0/(1+(K_{act}/[Ste5])$).

Structure Determination

Crystals of $Ste5_{582-786}$ were obtained by mixing 10 mg/mL of protein (1:1 vol:vol) with a solution containing 20% PEG 3350, 0.1 M $CaCl_2$, 25 mM Tris·HCl (pH 8.0), in hanging drops at 16 °C. Crystals grew as long rods that reached a maximum size in two days. The cryopreservant for X-ray data collection consisted of mother liquor supplemented with 25% glycerol. Diffraction data was collected in-house on a Rigaku R-Axis IV. Diffraction data was processed using XDS (19). Phases were obtained by molecular replacement with PHASER (20) using Ste5-ms (PDB 3FZE) as a search model. The resulting maps were of excellent quality and the additional density for the N-

terminal extension (residues 583-592) was readily visible in difference maps. The preliminary model obtained from molecular replacement was extended to include the additional residues, manually rebuilt in COOT (21), and refined using PHENIX (22). X-ray diffraction data and refinement statistics are shown in Table S4.

Structure Homology Modeling

In the model for Ste5 autoinhibition (Fig. 3D), structures of $Ste5_{582-786}$ (PDB 4F2H, this work) and Fus3 (PDB 2B9F (*23*)) are from experimental data. The structure of the Ste7 kinase domain was modeled from the structure of a homologous mammalian MAPKK (MKK7, PDB 2DYL). The Ste5 PH domain (residues 367-518) was modeled from the structure of a homologous PH domain from rat PLCδ (PDB 1MAI (*24*)). Homology models were generated using the threading program Phyre (*25*).

PH Domain Inhibition Experiments

For the *in trans* inhibition experiments, purified tag-free Ste5 PH domain (367-525) was exchanged into 25 mM Tris·HCl (pH 8.0), 100 mM NaCl, 2.5 mM $MgCl_2$, 0.05% IGEPAL, and 2 mM TCEP at 25 °C with a 7K MWCO Zebra 0.5 mL desalting column (Thermo Scientific). Varying concentrations of the PH domain were incubated with Ste5 VWA domain constructs (1 μM) for 30 minutes at room temperature prior to the addition of 50 nM Ste7EE and saturating (1 μM) Fus3 K42R. Reactions were initiated with 500 μM ATP at 25 °C and initial rates were determined by quantitative western blot as described above. The curves shown in Fig. 3E are described by the equation $k_{obs}=k_{cat}/(1+([PH]/K_I)$, where K_I was determined by curve fitting.

Fab Activation Experiments

For Fab activation experiments, purified SR13 Fab was exchanged into 25 mM Tris·HCl (pH 8.0), 100 mM NaCl, 2.5 mM $MgCl_2$, and 0.05% IGEPAL. SR13 Fab was incubated at varying concentrations with 1 μM full-length Ste5 for 30 minutes at room temperature before the addition of 50 nM Ste7EE and saturating (1 μM) Fus3. Reactions were initiated with 500 μM ATP at 25 °C and initial rates were determined by quantitative western blot as described above.

Reconstituted Vesicle Experiments

Phosphatidyl choline (PC, egg yolk), $PI(4,5)P_2$ (brain), and DGS-NTA(Ni) were purchased from Avanti. Unilamellar vesicles were generated by mixing PC with varying quantities of $PI(4,5)P_2$ and/or DGS-NTA(Ni) dissolved in chloroform in the molar ratios as indicated in Fig. 3G. Mixed lipids were dried under argon, placed under vacuum for 12 hours, and resuspended in 25 mM Tris·HCl (pH 8.0), 100 mM NaCl, and 2.5 mM $MgCl_2$ to a final concentration of 3.2 mM total lipid. Hydrated lipids were subjected to ten cycles of freezing in liquid nitrogen, thawing, and 1 min bath sonication. Lipids were then extruded through a 0.2 μM filter (Avanti). Approximate concentrations of an indicated lipid species were estimated as the mole fraction of the total lipid concentration divided by 2, assuming 50% of the total was on the inside layer of the vesicles. The resulting vesicles were stored at 4 °C and used in assays within five days of preparation.

For vesicle activation experiments, 500 nM (final reaction concentration) of the $Ste5_{His\text{-}PM\text{-}PH\text{-}VWA}$ construct (Fig. S13) was incubated with lipid vesicles (at ~160 μM lipid

concentration) in 25 mM Tris·HCl (pH 8.0), 100 mM NaCl, 2.5 mM $MgCl_2$, and 2 mM TCEP for 1 hour at 4 °C. The final lipid concentrations in reactions with 90:5:5 PC:PI(4,5)P_2:DGS-NTA(Ni) vesicles were approximately 144 μM PC, 8 μM PI(4,5)P_2, and 8 μM DGS-NTA(Ni). Following incubation, 50 nM Ste7EE and saturating (1 μM) Fus3 were added, the reactions were initiated with 500 μM ATP at 25 °C, and initial rates were determined by quantitative western blot as described above.

Figure S1. Exchange of the Ste7 MAPKK from the Ste5 scaffold protein is too fast for signaling pathway insulation by physical sequestration

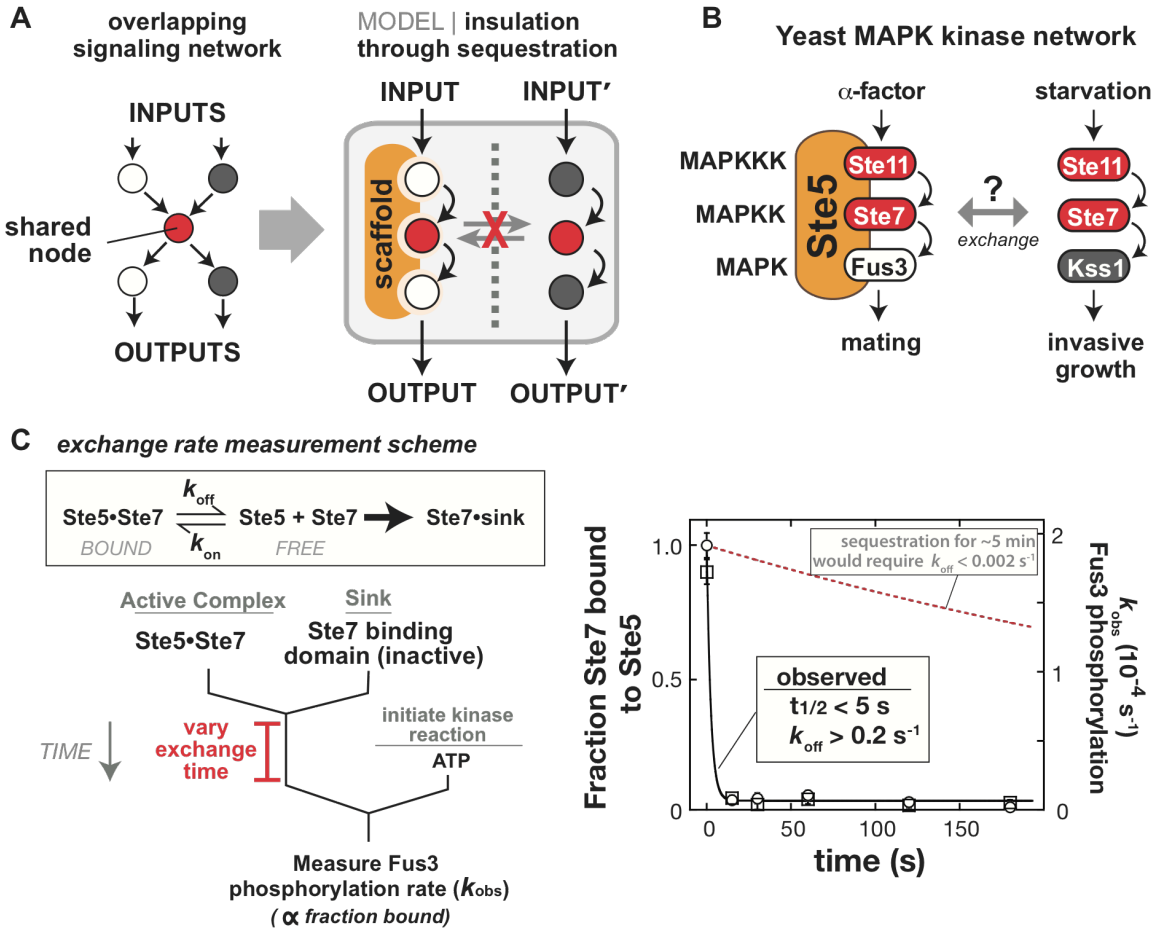

Fig. S1

(A) Signaling networks frequently share components. Physical sequestration by scaffold proteins has been proposed as a mechanism for pathway insulation by preventing exchange between distinct pools of signaling proteins.

(B) The yeast mating and invasive growth pathways are physiologically distinct input-output responses that share two common components – the MAPKKK Ste11 and the MAPKK Ste7. The Ste5 scaffold is essential for signaling through the mating pathway.

(C) The dissociation rate of the MAPKK Ste7 from the Ste5 scaffold protein is fast. Dissociation rates were measured with purified recombinant Ste5, the MAPKKK Ste11, the MAPK Fus3, and a constitutively active form of the MAPKK Ste7 (Ste7EE, bearing phosphomimic mutations in the Ste7 activation loop). To a preassembled Ste5-Ste7-Fus3 complex, an excess of a Ste7 binding domain (the "sink", a minimal Ste7 binding domain from Ste5 [residues 759-810]) was added to capture Ste7 as it dissociates from Ste5. After varying times, ATP was added, and the initial rate of Fus3 phosphorylation corresponds to the amount of Ste5-Ste7-Fus3 complex remaining at each timepoint. The observed k_{off} of 0.2 s^{-1} is a lower limit – dissociation occurs on a timescale faster than can be measured with mixing by hand. There was no detectable difference in the Ste5-Ste7 dissociation rate measured in the presence (○) or absence (□) of Ste11.

Figure S2. Ste5 has large effects on k_{cat} for Fus3 phosphorylation *in vitro*

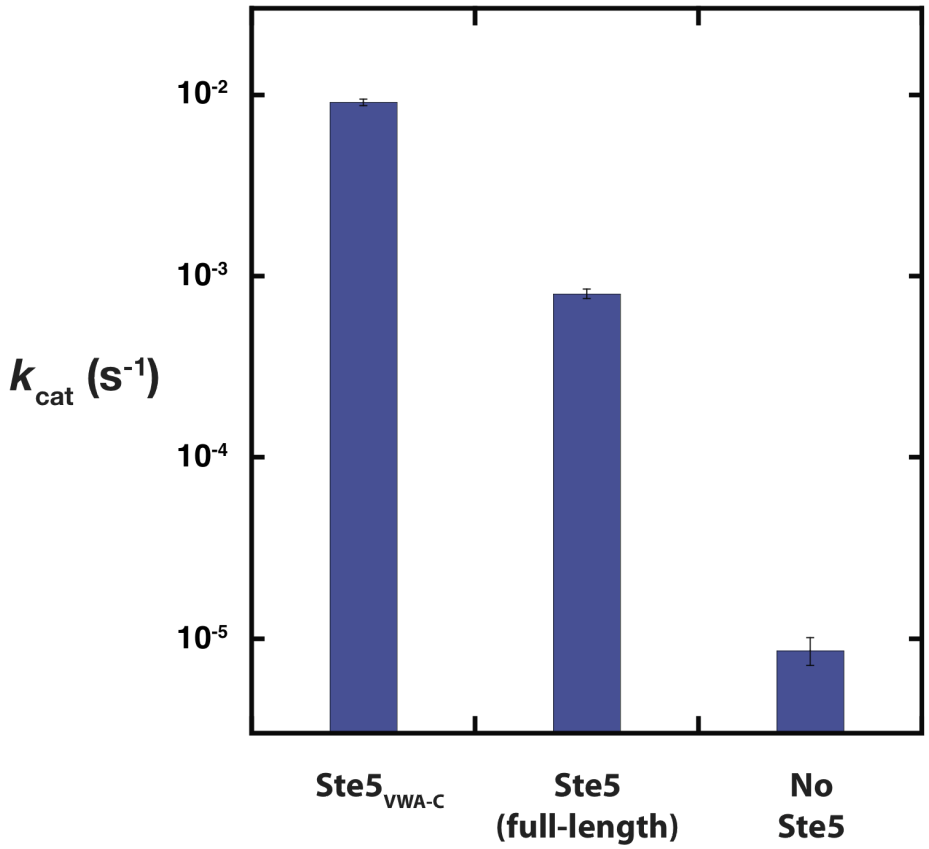

Fig. S2

Values of k_{cat} were measured for MBP-Ste7EE-catalyzed Fus3 phosphorylation in the absence of Ste5, with full-length Ste5, and with $Ste5_{VWA-C}$. $Ste5_{VWA-C}$ increases k_{cat} by ~10^3-fold, while full-length Ste5 increases k_{cat} by ~10^2-fold relative to the reaction in the absence of Ste5. The value of k_{cat} for MBP-Ste7EE in the absence of Ste5 of (8.6 ± 1.5) × 10^{-6} is ~10-fold greater than that measured previously with GST-Ste7EE-ND2 (*11*).

Figure S3. The VWA-C domain is a significantly better coactivator of Fus3 phosphorylation than full-length Ste5

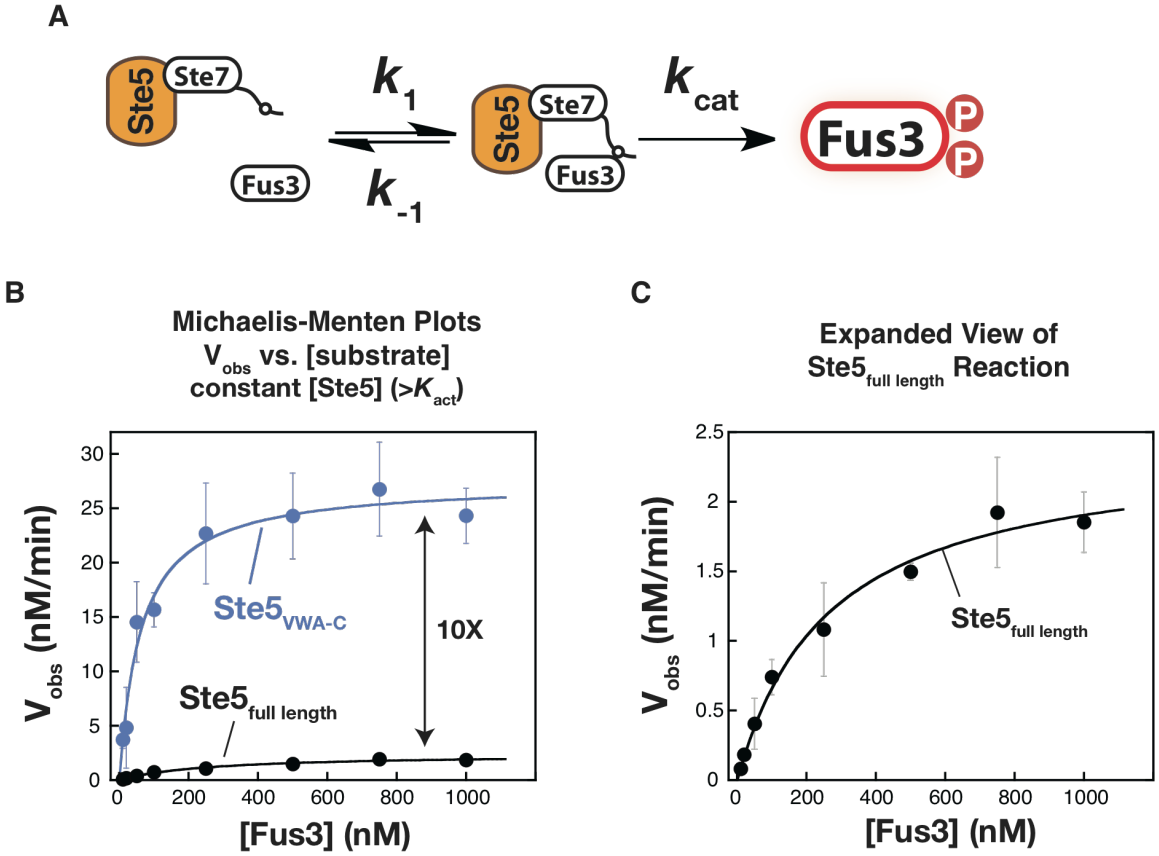

Fig. S3

(A) Kinetic scheme for Ste7→Fus3 phosphorylation in the presence of saturating Ste5.
(B) Michaelis-Menten plots (V_{obs} vs. [Fus3]) for MBP-Ste7EE with $Ste5_{VWA-C}$ and full-length Ste5.
(C) Expanded view of data for full-length Ste5. The value of k_{cat} is 10-fold slower for full-length Ste5 relative to the free VWA-C domain. The K_M is approximately 4-fold weaker for full-length Ste5, likely due to an additional binding site for the Fus3 substrate within the full-length Ste5, which can titrate out substrate (*15, 26*). Fitted values of kinetic constants are reported in Table S1.

Figure S4. Full-length Ste5 and the VWA-C domain have similar binding affinities for Ste7

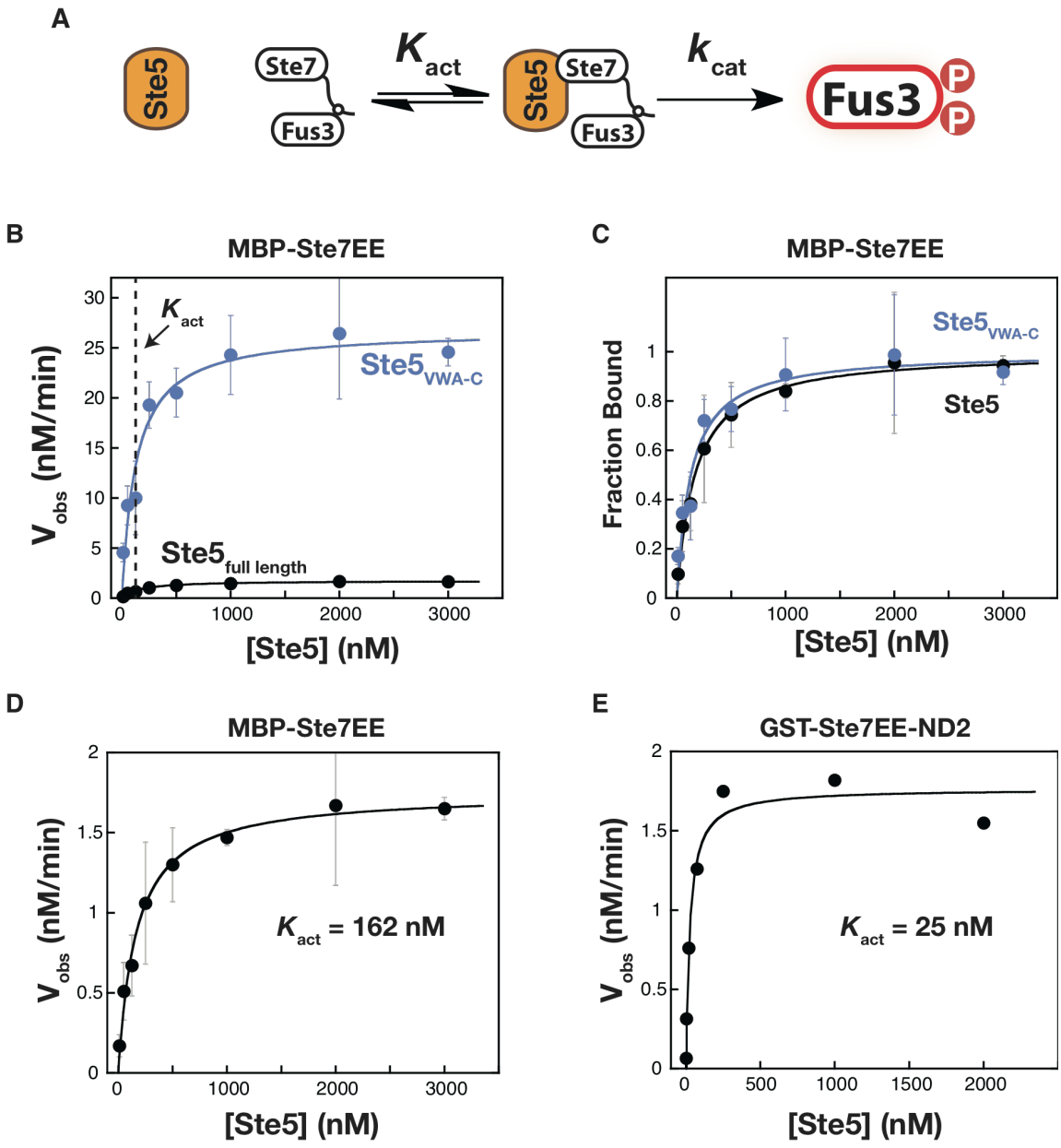

Fig. S4

(A) Kinetic scheme for Ste7→Fus3 phosphorylation at saturating Fus3 and varying concentrations of Ste5. K_{act} is the midpoint of the activation curve and corresponds to the dissociation constant for Ste5-Ste7.
(B) Plot of V_{obs} vs. [Ste5] for reactions of full-length Ste5 and $Ste5_{VWA-C}$ indicate that Ste5-Ste7 affinity binding is the same for these Ste5 constructs.
(C) Same as (B) but with the data normalized to demonstrate that the values of K_{act} for full-length Ste5 and $Ste5_{VWA-C}$ are indistinguishable.
(D and E) Comparison of K_{act} for MBP-Ste7EE and GST-Ste7EE-ND2 (with full-length Ste5, using 50 nM Ste7). Although GST-Ste7EE-ND2 was used in previous work (*11*), MBP-Ste7EE was used for all data reported in this work because it produced higher purity protein and avoids any potential artifacts arising from GST dimerization (*13, 14*). The value of K_{act} of 25 ± 7 nM for GST-Ste7EE-ND2 is an upper limit for K_{act} because it is approximately half of the concentration of Ste7 in the reaction and thus may reflect titration conditions. This value is substantially tighter than the value of 161 nM previously reported for GST-Ste7EE-ND2 binding to Ste5-ms (residues 593-786) (*11*) because full-length Ste5 contains the complete binding site for Ste7 that extends into the C-terminal tail (*27*). The tighter apparent binding by GST-Ste7EE-ND2 could be related to GST dimerization.

The ND2 designation indicates that the second, weak docking site for Fus3 has been removed (*15*). There is no difference in the behavior of Ste7EE and Ste7EE-ND2 for the kinetic parameters reported in this work.

Figure S5. Calibration of recognition of phospho-Fus3 and phospho-Kss1 on western blot allows for quantitative analysis of Fus3PP/Kss1PP levels *in vivo*

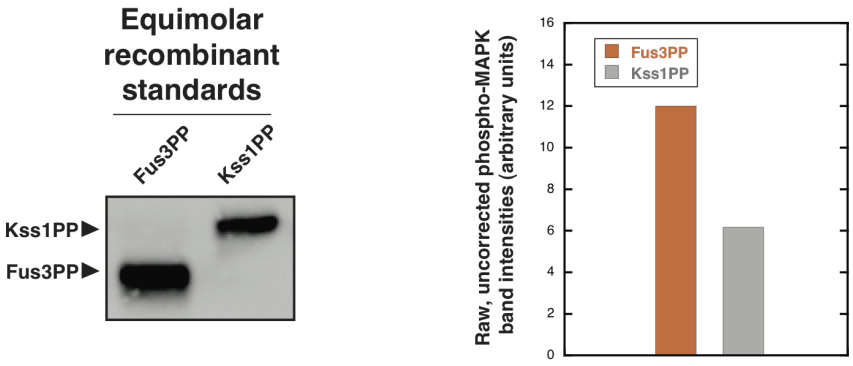

Fig. S5

The anti-phospho p44/p42 MAPK antibody (Cell Signaling Technology #4370) preferentially recognizes Fus3PP relative to Kss1PP. The average ratio of Fus3PP to Kss1PP is 2.1 ± 0.2 (± standard deviation, 10 measurements). Recombinant standards of Fus3PP and Kss1PP were prepared from proteins purified as described (*11*) and phosphorylated to completion with Ste7EE (and $Ste5_{VWA-C}$ for Fus3). The standards were loaded in equimolar quantities and analyzed by western blot using the anti-phospho p44/42 MAPK antibody (Cell Signaling Technology #4370). Band intensities were quantified using Li-Cor Odyssey 2.1 software.

Figure S6. The Ste5 VWA-C domain promotes misactivation of the mating MAPK Fus3 in response to starvation

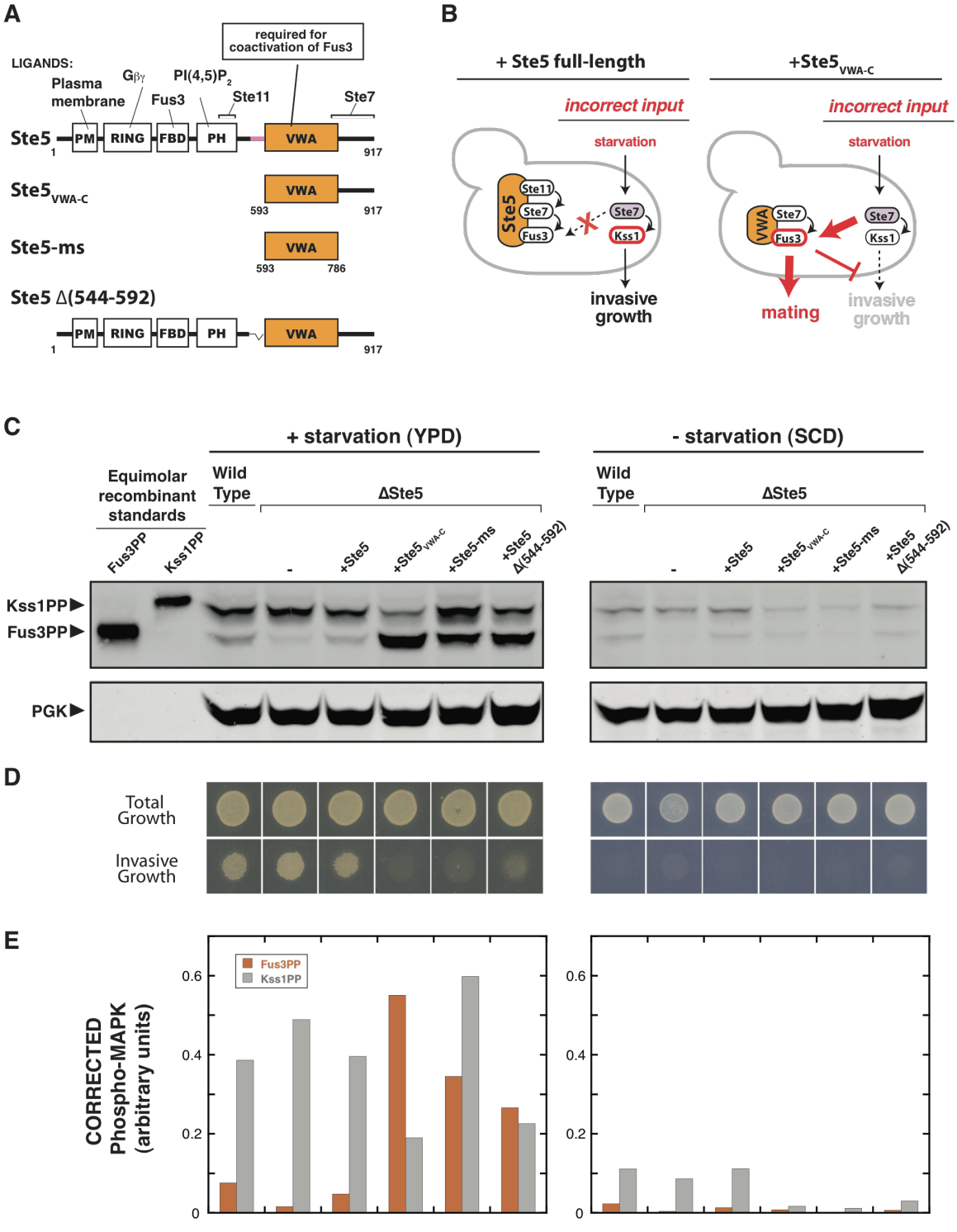

Fig. S6

(A) Schematic diagram of full-length Ste5 and truncation mutants. $Ste5_{VWA-C}$ is the minimal VWA domain plus the C-terminal tail that includes the complete Ste7 binding region (*27*). Ste5-ms is the minimal VWA domain (residues 593-786, previously described in (*11*)). Ste5Δ(544-592) is an internal truncation that is autoinhibited *in vitro* (Fig. 3A and 3B).

(B) Schematic for how starvation of yeast leads to misactivation of Fus3 when autoinhibition is disrupted in Ste5.

(C) Phosphorylation of MAP kinases in starvation conditions (growth on YPD plates) or unstarved (growth on SCD plates) monitored by anti-phospho western blotting. In the presence or absence of full-length Ste5, starvation activates Kss1. When Ste5 is replaced by $Ste5_{VWA-C}$, Ste5-ms, or Ste5Δ(544-592), starvation leads to Fus3 activation. Fus3 activation is strongest for $Ste5_{VWA-C}$. Active Fus3 has been reported to promote Kss1 dephosphorylation (*28*), leading to the decrease in Kss1 activation observed with $Ste5_{VWA-C}$. Phosphoglycerate kinase (PGK) is shown as a loading control for yeast lysates. All Ste5 constructs were expressed from the Ste5 promoter.

(D) Activation of Fus3 disrupts the invasive growth phenotype on YPD plates.

(E) Corrected relative amounts of Fus3PP and Kss1PP, performed as described in fig. S5 and normalized to PGK loading control.

Figure S7. Comparison of α-factor and starvation responses

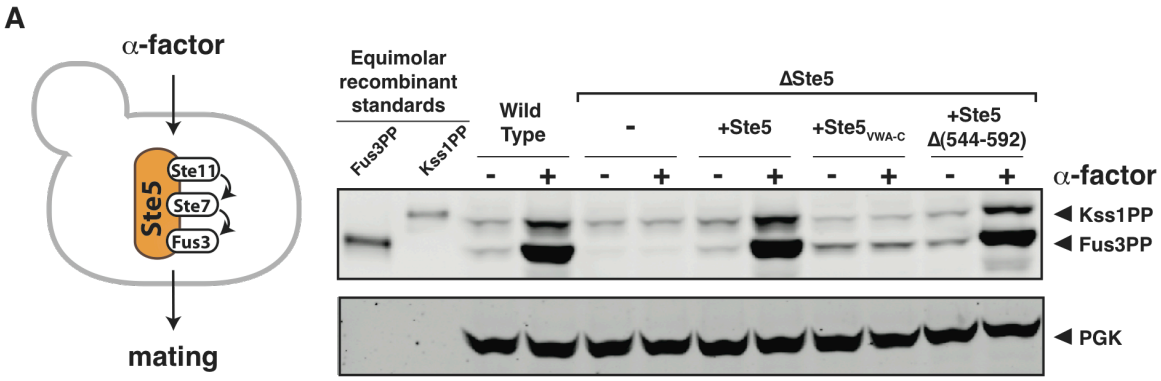

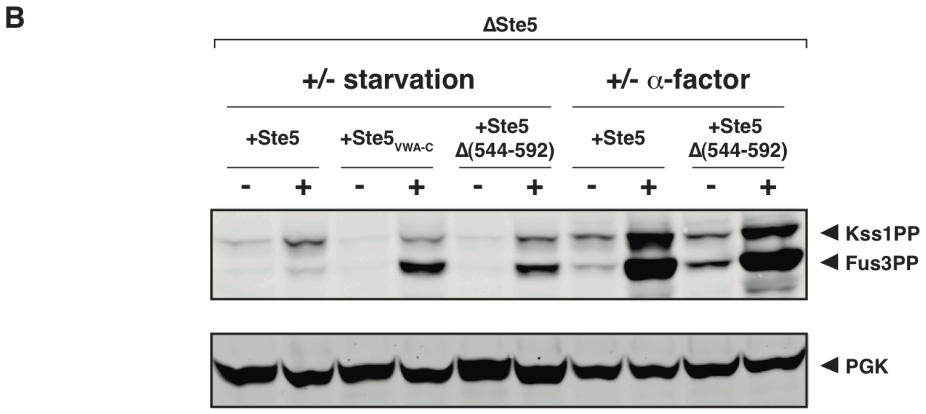

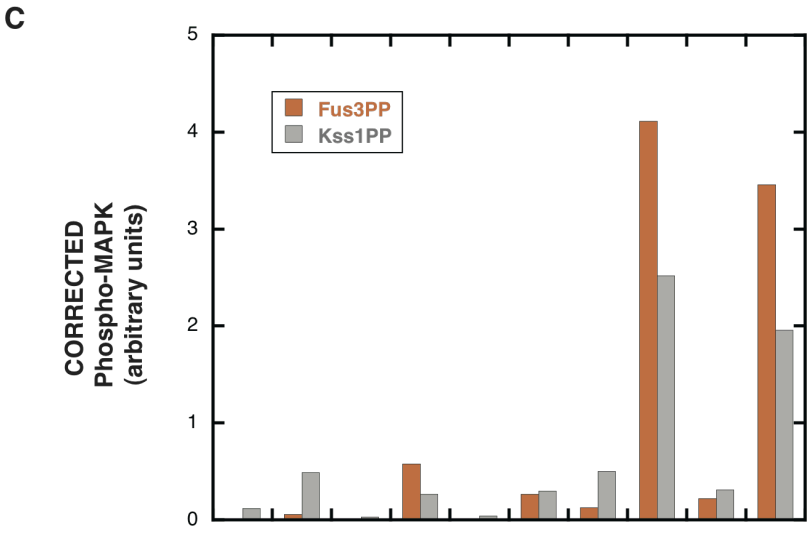

Fig. S7

(A) α-factor treatment activates the yeast mating MAP kinase pathway. Phosphorylation of MAP kinases in response to α-factor treatment monitored by anti-phospho western blotting. Cells with full-length Ste5 display robust activation of Fus3 and Kss1, and cells with Ste5Δ(544-592) are indistinguishable. The $Ste5_{VWA-C}$ construct lacks key domains necessary for membrane recruitment in response to α-factor (the PM (*29, 30*), RING (*31*), and PH (*32*) domains, see schematic in fig. S6) and for Ste11 binding (the PH domain (*27*)). All Ste5 constructs were expressed from the Ste5 promoter.

(B) Comparison of the starvation response and the mating response.

(C) Corrected relative amounts of Fus3PP and Kss1PP, performed as described in fig. S5 and normalized to PGK loading control. Cells produce significantly more MAPK phosphorylation in response to saturating α-factor (2 μM) than in response to starvation.

Figure S8. Ste5$_{VWA-C}$ promotes misactivation of the mating MAPK Fus3 in response to constitutively-active alleles of Ste11 and Ste7

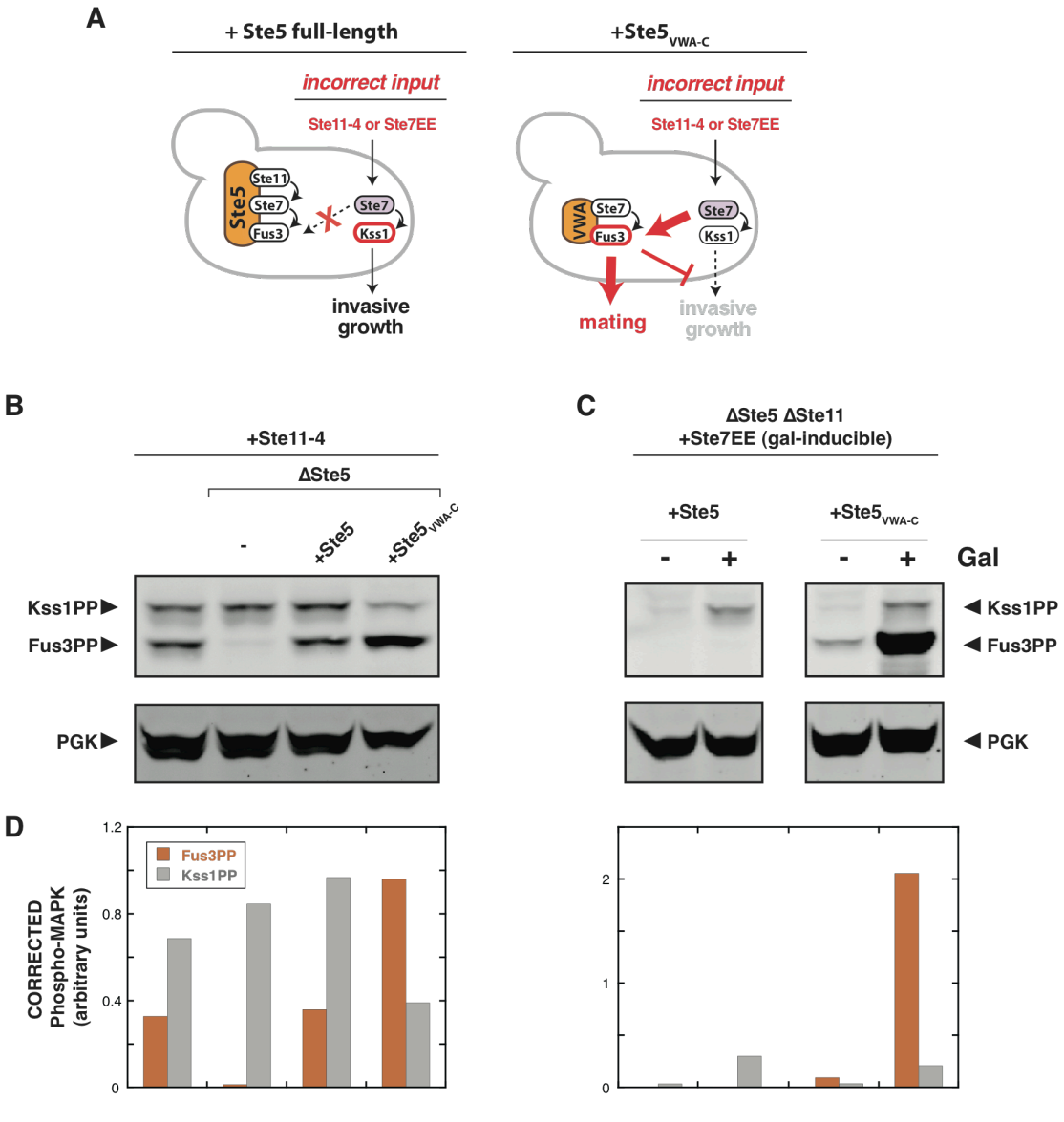

Fig. S8

(A) Schematic diagram for the effect of constitutive alleles of Ste11 and Ste7 in cells with full-length Ste5 and $Ste5_{VWA-C}$. Ste11-4 is a constitutively active allele of Ste11 (*33*) that preferentially activates Kss1 (*34, 35*). Ste7EE is a constitutively active allele of Ste7 (*11, 12*).

(B) Phosphorylation of MAP kinases monitored by anti-phospho western blotting. When Ste5 is replaced by $Ste5_{VWA-C}$, Ste11-4 leads to preferential Fus3 phosphorylation. The decrease in Kss1 phosphorylation is a consequence of active Fus3 promoting Kss1 dephosphorylation (*28*). Yeast cells were harvested from YPD liquid cultures grown to mid-log phase (OD_{600} = 0.5). PGK is shown as a loading control for yeast lysates. Ste5 and Ste11 constructs in this panel were expressed from their native promoters.

(C) Ste7EE preferentially phosphorylates Fus3 only in the presence of $Ste5_{VWA-C}$. To observe significant MAPK phosphorylation, Ste7EE was overexpressed from a galactose-inducible promoter, and Ste5 constructs were overexpressed from Adh promoters. These experiments were conducted in a strain background that is unable to activate the MAP kinase cascade (ΔSte5 ΔSte11) so that the observed MAPK phosphorylation is solely the product of Ste7EE.

(D) Corrected relative amounts of Fus3PP and Kss1PP, performed as described in fig. S5 and normalized to PGK loading control.

Figure S9. Detailed truncation mapping suggests that the PH domain of Ste5 interacts with and inhibits the VWA domain

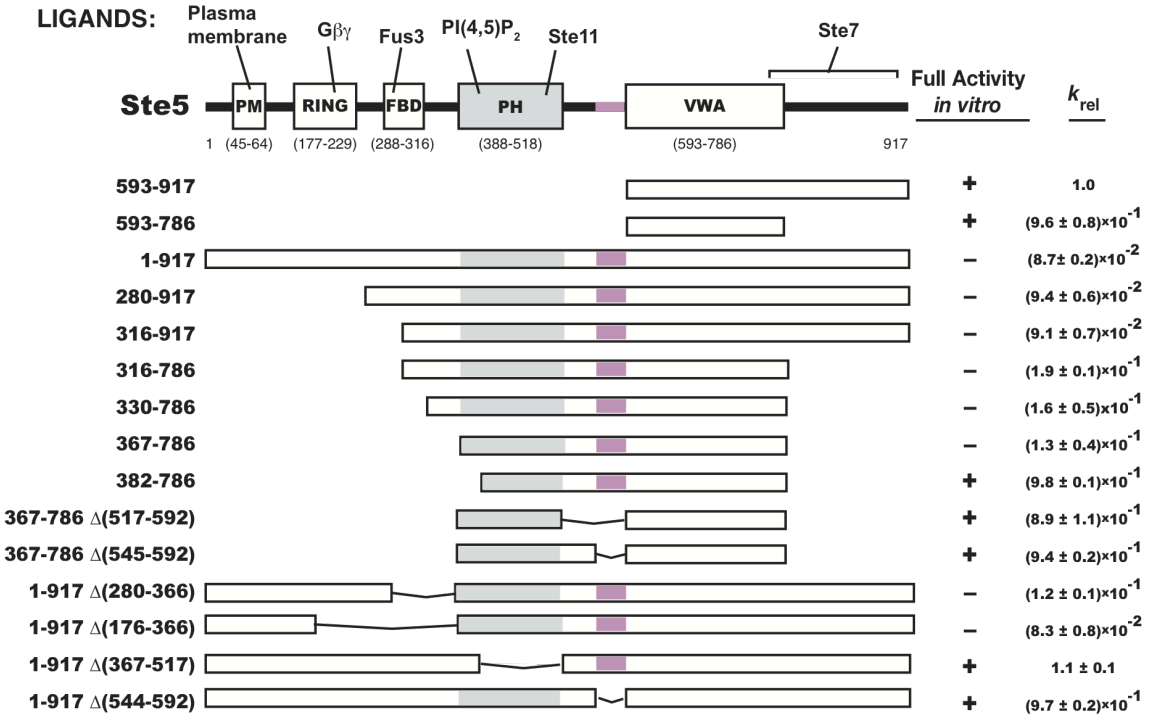

Fig. S9

Ste5 contains several well-characterized domains, including the PM helix, which facilitates membrane binding and mediates cell-cycle regulation of Ste5 activity (*29, 30*); the RING-H2 domain, which binds Gβ (Ste4) to localize Ste5 to the membrane when the pathway is stimulated (*31*); the Fus3-binding domain (FBD), which is not required for Fus3 activation but instead serves a feedback regulatory role (*26, 36*); the PH domain, which binds to phosphoinositol 4,5-bisphosphate ($PI(4,5)P_2$) to facilitate Ste5 membrane binding (*32*) and also includes the binding site for the MAPKKK Ste11 (*27*); and the VWA domain, which binds Ste7 and co-catalyzes Fus3 phosphorylation (*11*). The Ste7 binding site extends past the VWA domain into the C-terminal tail (*27*). We found that the PM-helix, RING-H2 domain, and FBD were dispensable for Ste5 autoinhibition. In contrast, truncation beyond the PH domain or internal deletion of the PH domain eliminated inhibition.

Truncation and internal deletions of Ste5 were purified to homogeneity and kinetic parameters for *in vitro* coactivator function were determined for each variant. A Ste5 variant was deemed autoinhibited if the observed k_{cat} (i.e. k_{obs} at saturating concentrations of Ste5 and Fus3) was within 2-fold of the full-length protein and deemed uninhibited if the observed k_{cat} was within 75% of the isolated VWA domain. Regions that result in loss of autoinhibition when disrupted in the context of the full-length protein are the PH/Ste11 binding domain (colored in gray), and an N-terminal extension of the VWA domain (colored in pink). The results suggest that the PH domain (367-525) and an N-terminal extension the VWA (544-592) are required to maintain Ste5 in an autoinhibited state.

Figure S10. The N-terminal extension of the Ste5 VWA domain displays a surface that is essential for strong binding of the PH domain to the VWA domain and inhibition of its Fus3 coactivator function

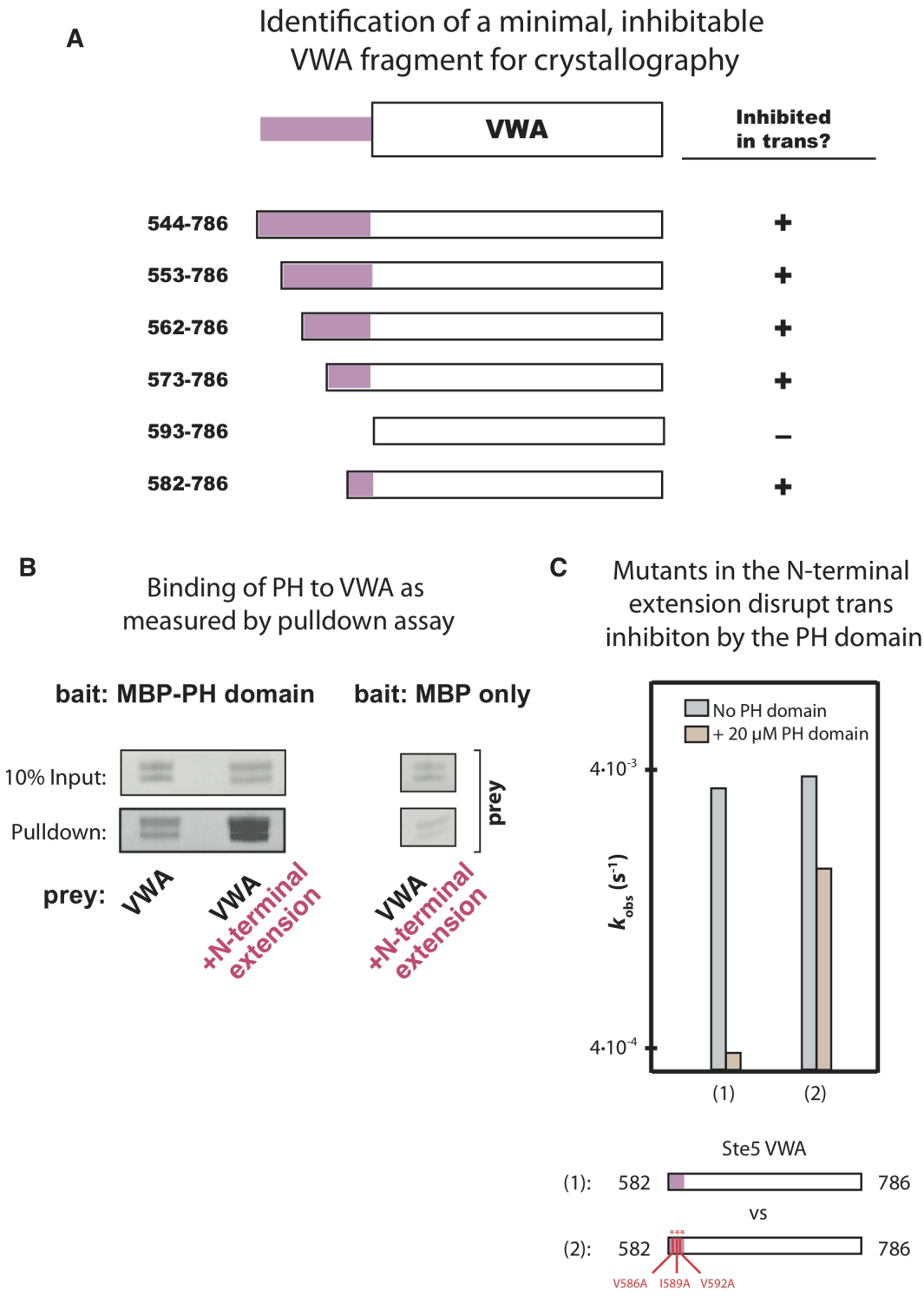

Fig. S10

(A) The minimal region of the N-terminal extension (residues 544-592) required for *in trans* inhibition by the PH domain was mapped to residues 582-592. This construct contains the minimal N-terminal extension (582-592) and the minimal VWA domain (593-786).

(B) 20 μM MBP-PH domain (367-525) was incubated with 20 μM of either VWA (593-786) or VWA+N-terminal extension (582-786) for 30 minutes at room-temperature before incubation with 15 μL of amylose resin at 4 °C for one hour. Samples were washed twice and eluted with 2X SDS loading buffer and analyzed by SDS-PAGE. The VWA domain runs as a doublet under these conditions. Only the VWA+N-terminal extension construct binds the PH domain.

(C) The coactivating activity of $Ste5_{582-786}$ (VWA with an N-terminal extension) or a construct bearing mutations along the surface of the N-terminal extension was measured in the absence or presence of 20 μM PH domain. Mutations in the N-terminal extension disrupt inhibition by the PH domain.

Figure S11. The SR13 Fab recognizes a PH domain-specific epitope and binds to the PH domain under native conditions

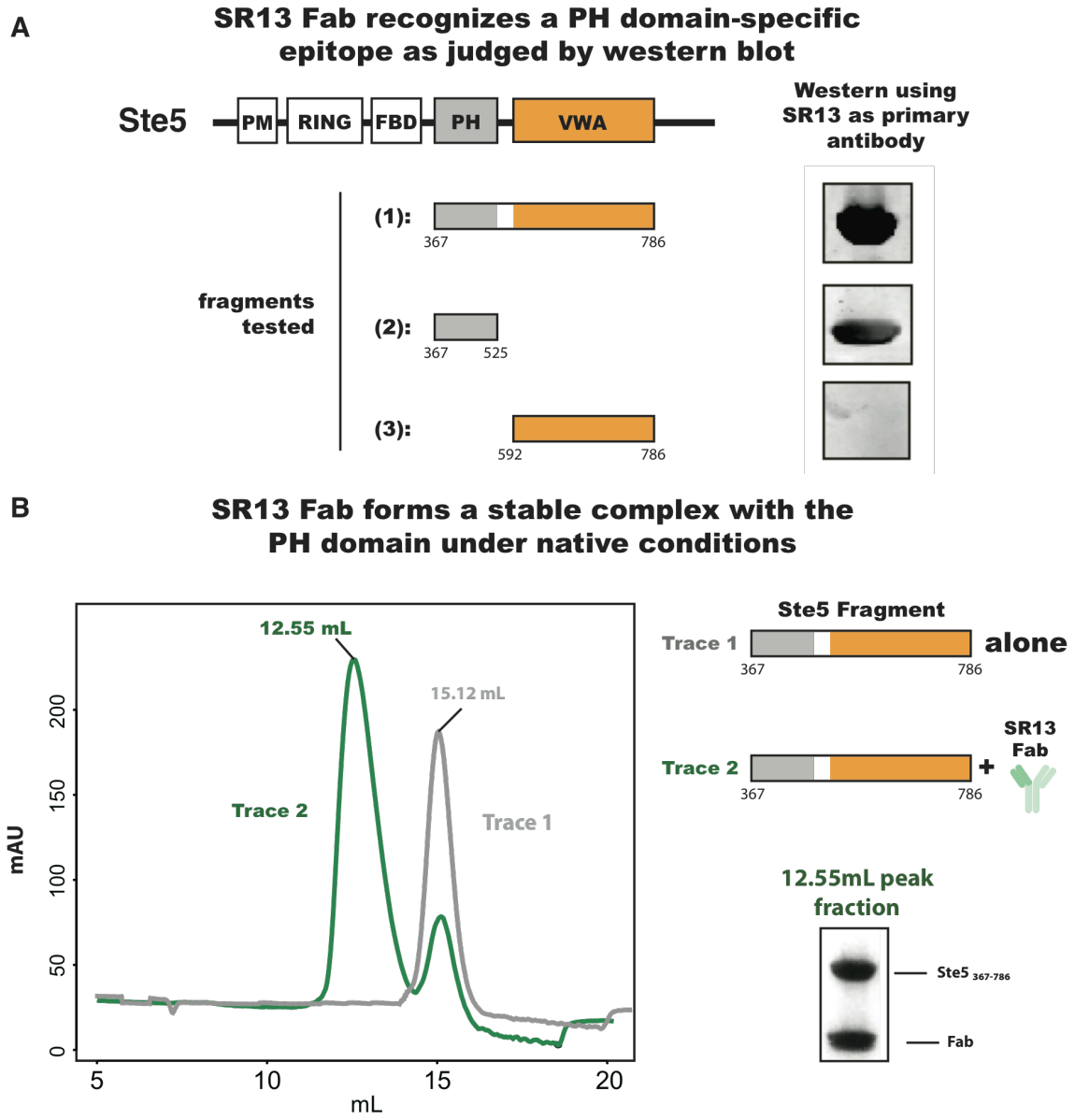

Fig. S11

(A) Western blot using the SR13 Fab as a primary antibody against a panel of Ste5 fragments, and using IRDye 800CW Goat Anti-Human IgG antibody (Li-Cor #926-32232) as the secondary antibody. SR13 recognizes the PH domain-containing fragments (1 and 2), but does not recognize a Ste5 fragment that lacks the PH domain (fragment 3). (B) Size-exclusion chromatograms (Superdex 200 10/300; GE Healthcare) of $Ste5_{367-786}$ (grey) or $Ste5_{367-786}$ in the presence of the SR13 Fab. $Ste5_{367-786}$ elutes at 15.12 mL whereas in the presence of the Fab a substantial portion elutes in an earlier, 12.55 mL peak. The peak fraction of the 12.55 mL peak was analyzed by SDS-PAGE and revealed approximately equivalent amounts of $Ste5_{367-786}$ and the Fab.

Figure S12. The "hyperactive" S770N Ste5 mutation disrupts autoinhibition of the Fus3 coactivator function of Ste5

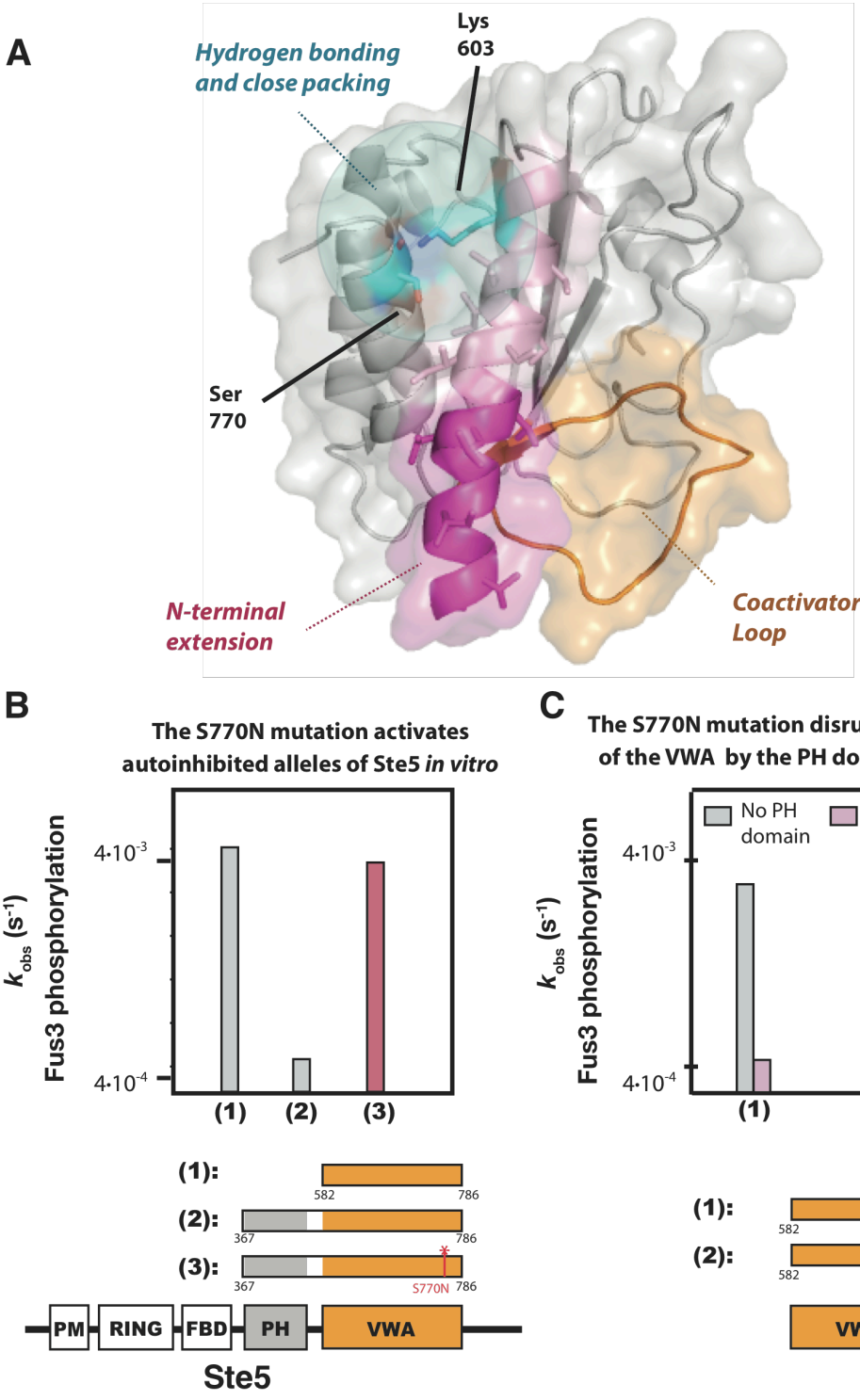

Fig. S12

Our model for inhibition is consistent with and suggests an explanation for the phenotype of a previously identified allele of Ste5 (S770N) that activates Fus3 in the absence of pheromone (*37, 38*). Ser770 lies on the same face of the VWA as the N-terminal helix, packs up against it, and orients its backbone carbonyl to make a hydrogen bond with Lys603. Disruption of this interaction in the S770N mutant likely destabilizes the binding site for the PH domain, and prevents Ste5 from adopting an autoinhibited conformation. Consistent with this prediction, we find that the S770N allele of Ste5 displays uninhibited coactivator activity *in vitro* and, furthermore, is inhibited less potently by the PH domain *in trans*.

(A) Structure of $Ste5_{582-786}$ highlighting the position of serine 770 and lysine 603 in blue, the entire N-terminal helix in pink, and the N-terminal extension required for high-affinity PH domain binding in magenta. The backbone carbonyl of serine 770 forms a hydrogen bond with lysine 603, and the side chain of serine 770 is closely packed with the N-terminal helix.
(B) Coactivator activity of $Ste5_{367-786}$ S770N at saturating [Ste5] (1 μM). Wild type $Ste5_{367-786}$ is autoinhibited. The activity of $Ste5_{367-786}$ S770N is similar to that of the isolated VWA domain.
(C) Coactivator activities of either wild type $Ste5_{582-786}$ or $Ste5_{582-786}$ (S770N) in the absence (grey) or presence (pink) of 10 μM PH domain inhibitor.

Figure S13. A minimal, autoinhibited membrane-binding Ste5 construct ($Ste5_{His\text{-}PM\text{-}PH\text{-}VWA}$) binds to PC:PI(4,5)$P_2$:DGS-NTA(Ni) vesicles

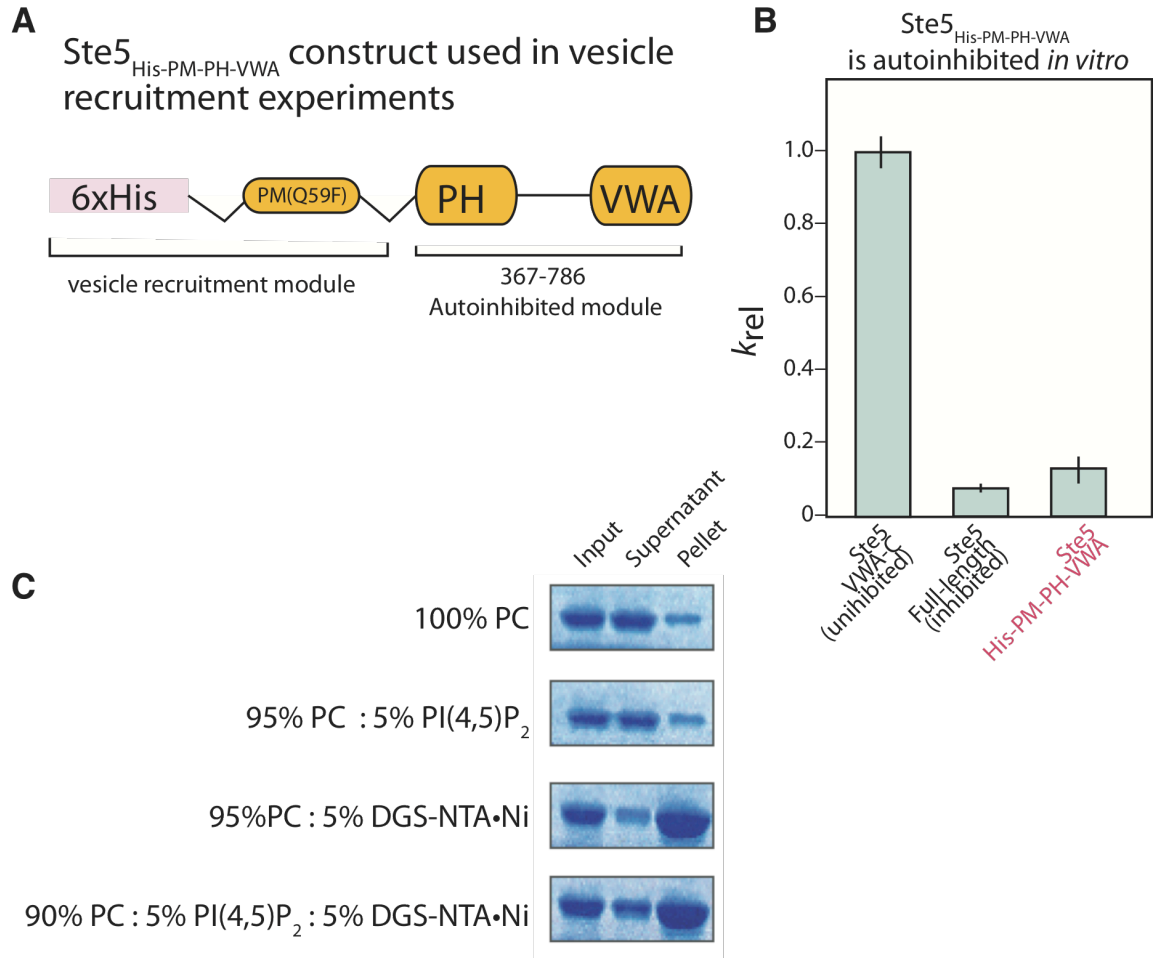

Fig. S13

(A) Schematic of the minimal, membrane-binding $Ste5_{His\text{-}PM\text{-}PH\text{-}VWA}$ construct used in vesicle binding and activation experiments. The construct contains a 6x-His tag to allow binding to DGS-NTA(Ni) lipids and a mutant form of the PM helix (Q59F; (*30*)) that raises the pI of the protein and improves binding to vesicles under assay conditions.

(B) The $Ste5_{His\text{-}PM\text{-}PH\text{-}VWA}$ construct is autoinhibited *in vitro*, similar to full-length Ste5. k_{rel} is the normalized value of k_{cat} (measured at saturating concentrations of Ste5 and Fus3).

(C) Binding of $Ste5_{His\text{-}PM\text{-}PH\text{-}VWA}$ to vesicles of varying PI(4,5)P_2 and DGS-NTA(Ni) composition. 10 μM protein was incubated with 400 μM vesicle for 1 hour at 4 °C and centrifuged for 1 hour at 51K RPM in a TLA-100 rotor. The amount of $Ste5_{His\text{-}PM\text{-}PH\text{-}VWA}$ in the input, supernatant, and pellet is shown as judged by Coomassie staining. No significant binding to PC or PC:PI(4,5)P_2 vesicles is observed, but significant binding is observed for vesicles with DGS-NTA(Ni). These vesicles recruit approximately half of the input protein under these conditions, which may explain why only partial activation of Ste5 is observed *in vitro* (Fig. 3G).

Figure S14. Oligomerization is not essential for relief of Ste5 autoinhibition

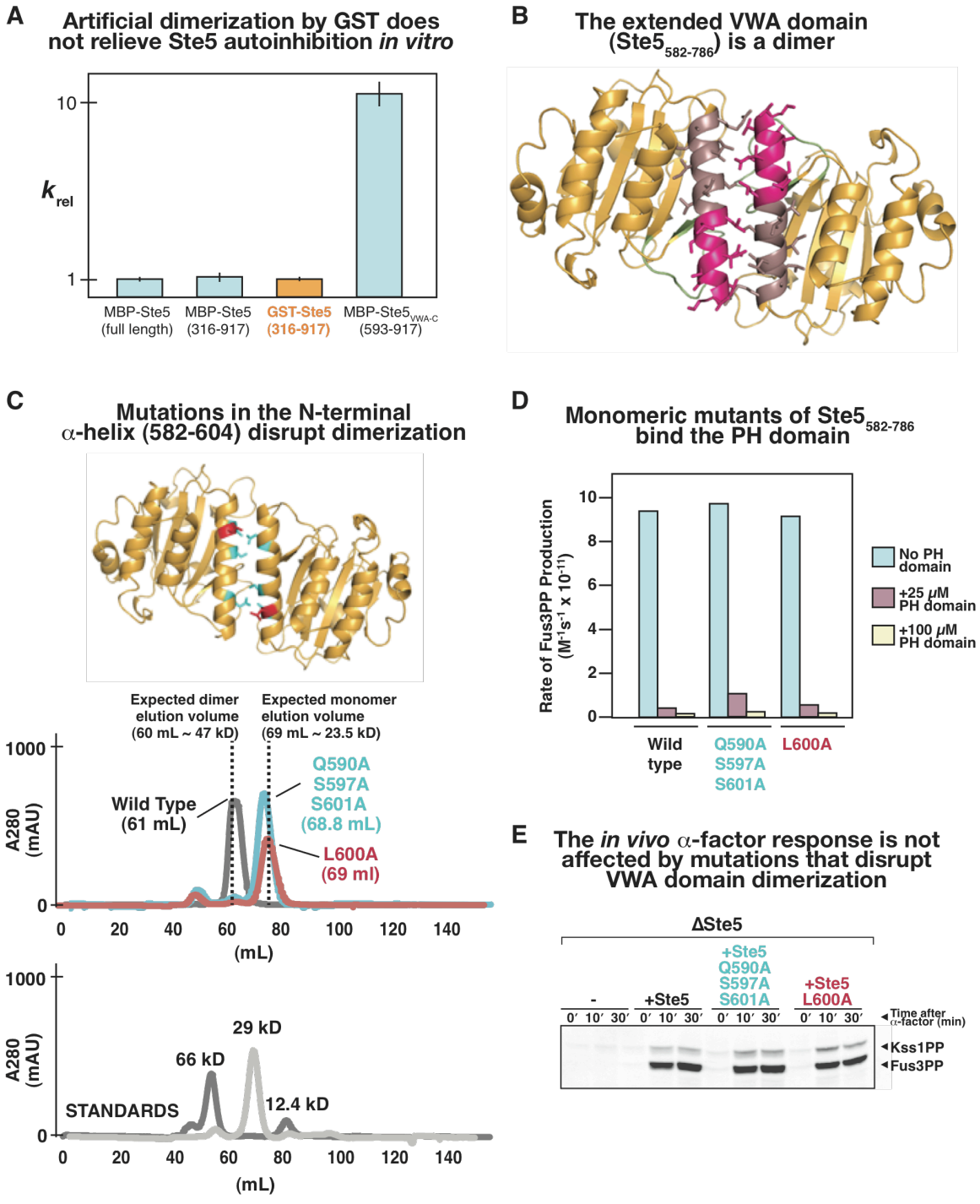

Fig. S14

Dimerization of Ste5 has been suggested to be important for mating pathway activation *in vivo* (*31, 37-40*), and this effect may act at the level of Ste11 activation (*31, 37-39*), upstream of activation of the mating MAPK Fus3. Although we cannot exclude a role for

Ste5 dimerization in the relief of autoinhibition of the VWA domain, we find no evidence supporting this possibility.

Key evidence supporting a role for dimerization of Ste5 in mating pathway activation comes from the observation that GST-tagged Ste5 leads to constitutive pathway activation in the absence of the mating input (α-factor) (*31, 37-39*). GST is known to form a dimer (*13, 14*). To test whether artificial dimerization of Ste5 with a GST tag could relieve autoinhibition of the VWA domain, we measured rate constants for a GST-tagged Ste5 construct *in vitro*, but no relief of autoinhibition was observed (Fig. S14A).

The extended Ste5 VWA domain ($Ste5_{582-786}$) is a dimer (Fig. S14B and C). Because the dimerization interface partially overlaps with features required for PH domain binding and inhibition (Fig. 3), dimerization along this interface could play a role in activating the protein. Specifically, dimerization may compete with autoinhibition by the PH domain and thereby stabilize the uninhibited conformation of Ste5. This model makes the prediction that if the dimerization interface is disrupted, Ste5 should remain inhibited even when cells are stimulated by the mating input. To test this possibility, we identified mutations that abolish dimerization (Fig. S14C) but were still subject to inhibition by the PH domain (Fig. S14D). We observed no significant changes in the mating response in yeast cells harboring these mutant versions of Ste5 (Fig. S14E), implying that dimerization along this interface is not essential for relief of Ste5 autoinhibition.

(A) The observed rate constant for Ste7EE-catalyzed phosphorylation of Fus3 with GST-$Ste5_{316-917}$ (we were unable to express full-length GST-Ste5) was indistinguishable from those for MBP-Ste5 or MBP-$Ste5_{316-917}$, constructs that are autoinhibited *in vitro* (Fig. 3A and S9). k_{cat} was measured at saturating concentrations of Ste5 and Fus3 and normalized to k_{cat} for MBP-$Ste5_{316-917}$.
(B) Structure of a novel crystallographic dimer of $Ste5_{582-786}$. The position of the N-terminal extension (residues 582-592) required for PH domain binding is colored in pink. The remaining portion of the α-helix that makes up the dimer interface (residues 593-604) is colored in burgundy.
(C) $Ste5_{582-786}$ is a dimer in solution, and dimer-interface mutants are monomers based on size-exclusion chromatograms (Superdex 75 16/60; GE Healthcare) for wild type (black) or mutants (cyan or red) of $Ste5_{582-786}$. Chromatograms for three molecular weight standards on the same column are also shown, and the position that a monomeric or dimeric form of $Ste5_{582-786}$ would be expected to run is indicated. Mutations that disrupt dimerization are shown on the structure and color-coded as cyan (Q590A, S597A, S601A) or red (L600A).
(D) Monomeric mutants of $Ste5_{582-786}$ retain the ability to bind to the PH domain. The PH domain of Ste5 inhibits the Fus3 co-activator function of both wild type and mutant forms of $Ste5_{582-786}$ *in trans*.
(E) Phosphorylation of MAP kinases in response to α-factor treatment monitored by anti-phospho western blotting. There is no significant difference between wild type Ste5 and dimerization-defective mutants. Ste5 constructs were expressed from the Ste5 promoter.

Figure S15. Pheromone triggers activation of the Ste5 scaffold protein

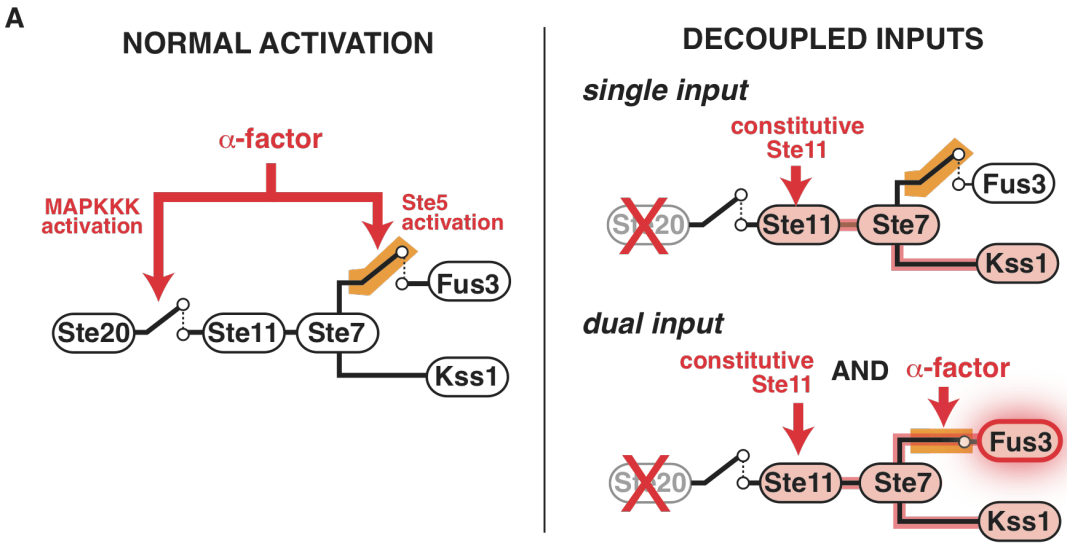

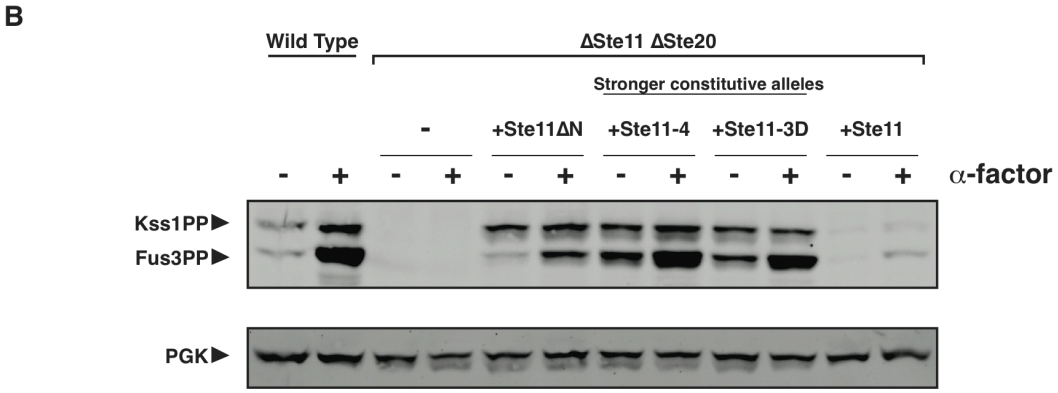

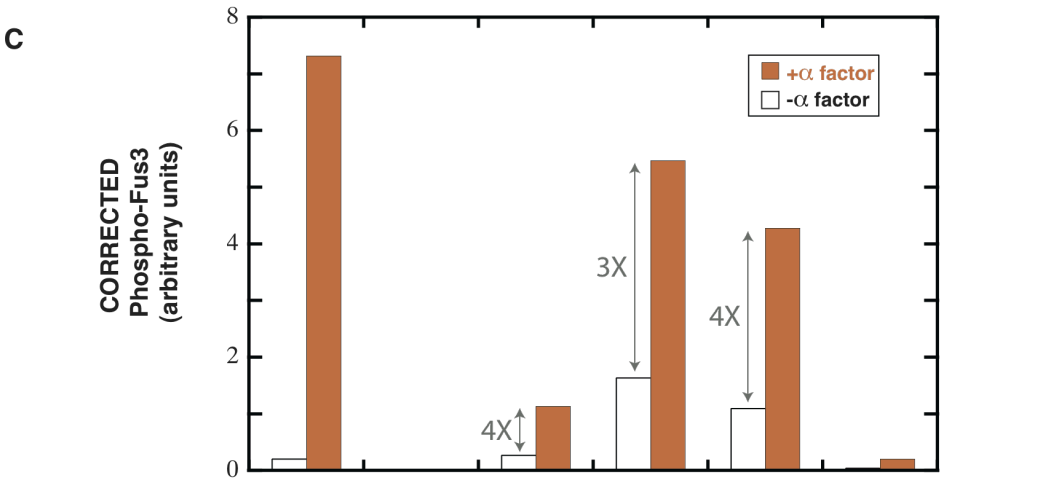

Fig. S15

(A) In wild type cells, α-factor treatment activates the MAPK cascade and the Ste5 scaffold protein. Decoupling the two functions of Ste5 can be accomplished by deleting the upstream kinase Ste20, which prevents activation of the MAPK cascade upon membrane recruitment of Ste5, and introducing a constitutively-active allele of Ste11.

(B) Phosphorylation of MAP kinases in response to α-factor monitored by anti-phospho western blotting. There is no α-factor response in a ΔSte11ΔSte20 strain, and restoring wild type Ste11 has no significant effect. Introduction of Ste11ΔN, Ste11-4, or Ste11-3D, which are constitutively-active alleles of the MAPKKK Ste11 (*33, 41, 42*), leads to significant Fus3 activation. Ste11ΔN is an amino-terminal truncation that renders the kinase constitutively-active (*41*) and also lacks the Ste5 binding site (*43*). This allele is therefore the most informative for assessing whether α-factor treatment activates Ste5 for the Ste7→Fus3 reaction (rather than the Ste11→Ste7 reaction). Ste11-4 and Ste11-3D contain point mutants that activate the kinase (*33, 42*). Ste11ΔN was overexpressed from an Adh1 promoter to compensate for the relatively weak activity of this allele, and all other Ste11 constructs were expressed from the Ste11 promoter (Table S3). The stronger basal Fus3 activation observed with Ste11-4 and Ste11-3D is likely to be a consequence of the comparatively strong constitutive activity of these alleles relative to that of Ste11ΔN.

(C) The change in Fus3PP levels +/- α-factor is similar for all three constitutive Ste11 alleles.

Table S1.

Kinetic constants for Fus3 phosphorylation reactions.[a]

	k_{cat} (s^{-1})	K_M (nM)	k_{cat}/K_M ($M^{-1}s^{-1}$)	K_{act} (nM)
$Ste5_{VWA-C}$	$(9.1 \pm 0.4) \times 10^{-3}$	62 ± 11	$(1.5 \pm 0.3) \times 10^{5}$	127 ± 32
Ste5 (full-length)	$(8.0 \pm 0.5) \times 10^{-4}$	263 ± 44	$(3.0 \pm 0.5) \times 10^{3}$	165 ± 21

[a] See Fig. 2 for data and Methods for kinetic models used to fit the data. The k_{cat} with $Ste5_{VWA-C}$ is 10-fold larger than with full-length Ste5, while K_{act} is unchanged. The K_M is approximately 4-fold weaker for full-length Ste5, but this is likely due to the presence of an additional binding site for the Fus3 substrate within the full-length Ste5 which can titrate out substrate (*15, 26*). Standard errors are from non-linear least squares fits to the initial rate data.

Table S2.

Yeast strains used in this study.[a]

Strain	Description	Genotype
F1950	Σ1278b derivative	*MAT***a** *ura3 leu2 trp1 his3*
JZ003	F1950 ΔSte5	*MAT***a** *ste5::kan^R ura3 leu2 trp1 his3*
JZ011	F1950 ΔSte5 ΔSte2	*MAT***a** *ste5::kan^R ste2::nat^R ura3 leu2 trp1 his3*
JZ012	F1950 ΔSte5 ΔSte11	*MAT***a** *ste5::kan^R ste11::nat^R ura3 leu2 trp1 his3*
JZ018	F1950 ΔSte11 ΔSte20	*MAT***a** *ste11::nat^R Ste20::hph^R ura3 leu2 trp1 his3*
YM2369	Σ1278b derivative	*MAT*α *his1*

[a] Strains F1950 and YM2369 were provided by H. Madhani (*1*).

Table S3.

Yeast expression plasmids used in this study.[a]

Plasmid	Parent Vector	Marker	Promoter[b]	Gene
pJZ525	pNH605	*leu2*	*pSte5*	Ste5
pJZ526	pNH605	*leu2*	*pSte5*	Ste5-ms (593-786)
pJZ550	pNH605	*leu2*	*pSte5*	$Ste5_{VWA-C}$ (593-917)
pJZ559[c]	pNH605	*leu2*	*pSte5*	Ste5Δ(544-592)
pJZ584	pNH605	*leu2*	*pAdh*	Ste5
pJZ586	pNH605	*leu2*	*pAdh*	$Ste5_{VWA-C}$ (593-917)
pJZ577[d]	pSV606	*ura3*	*pGal*	Ste7EE
pJZ527	pNH603	*his3*	*pSte11*	Ste11
pJZ528[d]	pNH603	*his3*	*pSte11*	Ste11-4
pJZ529[d]	pNH603	*his3*	*pSte11*	Ste11-3D
pJZ590[d]	pNH603	*his3*	*pAdh1*	Ste11ΔN
pSC179	pNH605	*leu2*	*pSte5*	$Ste5_{Q590A, S597A, S601A}$
pSC185	pNH605	*leu2*	*pSte5*	$Ste5_{L600A}$

[a] These vectors integrate a single copy into the yeast genome at the corresponding auxotrophic marker site (see Methods).

[b] Ste5 and Ste11 promoters consist of 500 bases immediately upstream of the start site for the corresponding gene. The Adh1 promoter consists of 1500 bases immediately upstream of the Adh1 gene. The Gal promoter consists of 689 bases immediately upstream of the Gal10 gene.

[c] The deleted residues in this Ste5 construct were replaced with a 5X(GAGS) linker.

[d] Constitutively active alleles of Ste7 (*11, 12*) and Ste11 (*33, 41, 42*) have been described previously.

Table S4.

Crystallographic Statistics for $Ste5_{582-786}$ structure (PDB ID: 4F2H).

Data Statistics	**Ste5 582-786**
Space Group	I222
Unit Cell	63.84 87.35 100.10 90.000 90.000 90.000
Wavelength	1.5418 Å
Resolution (last shell)	19.7-3.19 Å (3.28-3.19 Å)
Unique Reflections	25304
Redundancy	5.75 (4.91)
Completeness	90% (90%)
I/ σ	25.4 (10.56)
R_{sym}	10.9% (23.6%)
Refinement Statistics	
Resolution Range	19.7-3.19 Å
Reflections Used Work (Test)	4395 (220)
R_{cryst}/R_{free}	18.3%/ 25.7%
Overall figure of merit	.81333
r.m.s.d. bonds/angles	.043 Å /1.241º
Average B factor	34.25 $Å^2$
Ramachandran Analysis (Preferred / Allowed)	93.12% (6.35%)

r.m.s.d. is the root-mean squared deviation from ideal geometry.

$R_{sym} = \Sigma_{hkl}\Sigma_i |I_{hkl,i} - \langle I_{hkl,i}\rangle|/\Sigma_{hkl}\Sigma_i|I_{hkl,i}|$

R_{cyst} and $R_{free} = \Sigma|F_{obs} - F_{calc}|/\Sigma|F_{obs}|$. F_{obs} and F_{calc} are observed and calculated structure factors. R_{free} is calculated from a set of randomly chosen 5% of reflections, and R_{cyst} is calculated with the remaining 95% of reflections.

References

1. M. A. Schwartz, H. D. Madhani, Control of MAPK signaling specificity by a conserved residue in the MEK-binding domain of the yeast scaffold protein Ste5. *Curr. Genet.* **49**, 351 (2006).
2. J. G. Cook, L. Bardwell, J. Thorner, Inhibitory and activating functions for MAPK Kss1 in the *S. cerevisiae* filamentous-growth signalling pathway. *Nature* **390**, 85 (1997).
3. R. L. Roberts, G. R. Fink, Elements of a single MAP kinase cascade in *Saccharomyces cerevisiae* mediate two developmental programs in the same cell type: mating and invasive growth. *Gene Dev* **8**, 2974 (1994).
4. P. J. Cullen, G. F. Sprague, Jr., Glucose depletion causes haploid invasive growth in yeast. *Proc. Natl. Acad. Sci. U.S.A.* **97**, 13619 (2000).
5. M. S. Longtine *et al.*, Additional modules for versatile and economical PCR-based gene deletion and modification in *Saccharomyces cerevisiae*. *Yeast* **14**, 953 (1998).
6. A. L. Goldstein, J. H. McCusker, Three new dominant drug resistance cassettes for gene disruption in *Saccharomyces cerevisiae*. *Yeast* **15**, 1541 (1999).
7. R. D. Gietz, R. H. Schiestl, High-efficiency yeast transformation using the LiAc/SS carrier DNA/PEG method. *Nat. Protocols* **2**, 31 (2007).
8. R. S. Sikorski, P. Hieter, A system of shuttle vectors and yeast host strains designed for efficient manipulation of DNA in *Saccharomyces cerevisiae*. *Genetics* **122**, 19 (1989).
9. T. von der Haar, Optimized protein extraction for quantitative proteomics of yeasts. *PLoS One* **2**, e1078 (2007).
10. G. F. Sprague, Jr., Assay of yeast mating reaction. *Methods Enzymol.* **194**, 77 (1991).
11. M. Good, G. Tang, J. Singleton, A. Remenyi, W. A. Lim, The Ste5 scaffold directs mating signaling by catalytically unlocking the Fus3 MAP kinase for activation. *Cell* **136**, 1085 (2009).
12. S. Maleri *et al.*, Persistent activation by constitutive Ste7 promotes Kss1-mediated invasive growth but fails to support Fus3-dependent mating in yeast. *Mol. Cell. Biol.* **24**, 9221 (2004).
13. J. Walker, P. Crowley, A. D. Moreman, J. Barrett, Biochemical properties of cloned glutathione *S*-transferases from *Schistosoma mansoni* and *Schistosoma japonicum*. *Mol. Biochem. Parasitol.* **61**, 255 (1993).
14. R. Fabrini *et al.*, Monomer-dimer equilibrium in glutathione transferases: a critical re-examination. *Biochemistry* **48**, 10473 (2009).
15. A. Remenyi, M. C. Good, W. A. Lim, Docking interactions in protein kinase and phosphatase networks. *Curr. Opin. Struct. Biol.* **16**, 676 (2006).
16. F. A. Fellouse *et al.*, High-throughput generation of synthetic antibodies from highly functional minimalist phage-displayed libraries. *J. Mol. Biol.* **373**, 924 (2007).
17. F. A. Fellouse, S. S. Sidhu, in *Making and using antibodies,* G. C. Howard, M. R. Kaser, Eds. (CRC Press, Boca Raton, FL, 2007), pp. 157-180.

18. T. A. Kunkel, J. D. Roberts, R. A. Zakour, Rapid and efficient site-specific mutagenesis without phenotypic selection. *Methods Enzymol.* **154**, 367 (1987).
19. W. Kabsch, XDS. *Acta Cryst.* **D66**, 125 (2010).
20. A. J. McCoy *et al.*, Phaser crystallographic software. *J. Appl. Cryst.* **40**, 658 (2007).
21. P. Emsley, B. Lohkamp, W. G. Scott, K. Cowtan, Features and development of Coot. *Acta Cryst.* **D66**, 486 (2010).
22. P. D. Adams *et al.*, PHENIX: a comprehensive Python-based system for macromolecular structure solution. *Acta Cryst.* **D66**, 213 (2010).
23. A. Remenyi, M. C. Good, R. P. Bhattacharyya, W. A. Lim, The role of docking interactions in mediating signaling input, output, and discrimination in the yeast MAPK network. *Mol. Cell* **20**, 951 (2005).
24. K. M. Ferguson, M. A. Lemmon, J. Schlessinger, P. B. Sigler, Structure of the high affinity complex of inositol trisphosphate with a phospholipase C pleckstrin homology domain. *Cell* **83**, 1037 (1995).
25. L. A. Kelley, M. J. Sternberg, Protein structure prediction on the Web: a case study using the Phyre server. *Nat. Protocols* **4**, 363 (2009).
26. R. P. Bhattacharyya *et al.*, The Ste5 scaffold allosterically modulates signaling output of the yeast mating pathway. *Science* **311**, 822 (2006).
27. C. Inouye, N. Dhillon, T. Durfee, P. C. Zambryski, J. Thorner, Mutational analysis of STE5 in the yeast *Saccharomyces cerevisiae*: Application of a differential interaction trap assay for examining protein-protein interactions. *Genetics* **147**, 479 (1997).
28. W. Sabbagh, L. J. Flatauer, A. J. Bardwell, L. Bardwell, Specificity of MAP kinase signaling in yeast differentiation involves transient versus sustained MAPK activation. *Mol. Cell* **8**, 683 (2001).
29. S. C. Strickfaden *et al.*, A mechanism for cell-cycle regulation of MAP kinase signaling in a yeast differentiation pathway. *Cell* **128**, 519 (2007).
30. M. J. Winters, R. E. Lamson, H. Nakanishi, A. M. Neiman, P. M. Pryciak, A membrane binding domain in the Ste5 scaffold synergizes with Gβγ binding to control localization and signaling in pheromone response. *Mol. Cell* **20**, 21 (2005).
31. C. Inouye, N. Dhillon, J. Thorner, Ste5 RING-H2 domain: Role in Ste4-promoted oligomerization for yeast pheromone signaling. *Science* **278**, 103 (1997).
32. L. S. Garrenton, S. L. Young, J. Thorner, Function of the MAPK scaffold protein, Ste5, requires a cryptic PH domain. *Gene Dev* **20**, 1946 (2006).
33. B. J. Stevenson, N. Rhodes, B. Errede, G. F. Sprague, Jr., Constitutive mutants of the protein kinase STE11 activate the yeast pheromone response pathway in the absence of the G protein. *Genes Dev.* **6**, 1293 (1992).
34. L. J. Flatauer, S. F. Zadeh, L. Bardwell, Mitogen-activated protein kinases with distinct requirements for Ste5 scaffolding influence signaling specificity in *Saccharomyces cerevisiae*. *Mol. Cell. Biol.* **25**, 1793 (2005).
35. J. Andersson, D. M. Simpson, M. S. Qi, Y. M. Wang, E. A. Elion, Differential input by Ste5 scaffold and Msg5 phosphatase route a MAPK cascade to multiple outcomes. *EMBO J.* **23**, 2564 (2004).

36. M. K. Malleshaiah, V. Shahrezaei, P. S. Swain, S. W. Michnick, The scaffold protein Ste5 directly controls a switch-like mating decision in yeast. *Nature* **465**, 101 (2010).
37. R. E. Lamson, S. Takahashi, M. J. Winters, P. M. Pryciak, Dual role for membrane localization in yeast MAP kinase cascade activation and its contribution to signaling fidelity. *Curr. Biol.* **16**, 618 (2006).
38. C. Sette, C. J. Inouye, S. L. Stroschein, P. J. Iaquinta, J. Thorner, Mutational analysis suggests that activation of the yeast pheromone response mitogen-activated protein kinase pathway involves conformational changes in the Ste5 scaffold protein. *Mol. Biol. Cell* **11**, 4033 (2000).
39. Y. Wang, E. A. Elion, Nuclear export and plasma membrane recruitment of the Ste5 scaffold are coordinated with oligomerization and association with signal transduction components. *Mol. Biol. Cell* **14**, 2543 (2003).
40. D. Yablonski, I. Marbach, A. Levitzki, Dimerization of Ste5, a mitogen-activated protein kinase cascade scaffold protein, is required for signal transduction. *Proc. Natl. Acad. Sci. U.S.A.* **93**, 13864 (1996).
41. B. R. Cairns, S. W. Ramer, R. D. Kornberg, Order of action of components in the yeast pheromone response pathway revealed with a dominant allele of the STE11 kinase and the multiple phosphorylation of the STE7 kinase. *Genes Dev.* **6**, 1305 (1992).
42. F. van Drogen *et al.*, Phosphorylation of the MEKK Ste11p by the PAK-like kinase Ste20p is required for MAP kinase signaling *in vivo*. *Curr. Biol.* **10**, 630 (2000).
43. G. Jansen, F. Buhring, C. P. Hollenberg, M. Ramezani Rad, Mutations in the SAM domain of *STE50* differentially influence the MAPK-mediated pathways for mating, filamentous growth and osmotolerance in *Saccharomyces cerevisiae*. *Mol. Genet. Genomics* **265**, 102 (2001).